LEVEL II

R-1388

MATERIALS RESEARCH FOR ADVANCED INERTIAL INSTRUMENTATION

TASK 1: DIMENSIONAL STABILITY OF GYRO STRUCTURAL MATERIALS

TECHNICAL REPORT NO. 2
FOR THE PERIOD
1 OCTOBER 1978 — 30 SEPTEMBER 1979

BY

J. McCARTHY and F. PETRI

Prepared for the Office of Naval Research, Department of the Navy, under Contract N00014-77-C-0388.

The Charles Stark Draper Laboratory, Inc.
Cambridge, Massachusetts 02139

UNCLASSIFIED

SECURITY CLASSIFICATION OF THIS PAGE (When Data Entered)

REPORT DOCUMENTATION PAGE

READ INSTRUCTIONS BEFORE COMPLETING FORM

1. REPORT NUMBER: Technical Report No. 2	2. GOVT ACCESSION NO.: AD-A089598
3. RECIPIENT'S CATALOG NUMBER:	
4. TITLE (and Subtitle): Materials Research for Advanced Inertial Instrumentation Task 1: Dimensional Stability of Gyro Structural Materials	5. TYPE OF REPORT & PERIOD COVERED: Research Report 10/1/78 - 9/30/79
	6. PERFORMING ORG. REPORT NUMBER: R-1388
7. AUTHOR(s): J. McCarthy and F. Petri	8. CONTRACT OR GRANT NUMBER(s): N00014-77-C-0388
9. PERFORMING ORGANIZATION NAME AND ADDRESS: The Charles Stark Draper Laboratory, Inc. 555 Technology Square Cambridge, Massachusetts 02139	10. PROGRAM ELEMENT, PROJECT, TASK AREA & WORK UNIT NUMBERS:
11. CONTROLLING OFFICE NAME AND ADDRESS: Office of Naval Research Department of the Navy 800 N. Quincy Street, Arlington, Virginia 22217	12. REPORT DATE: June 1980
	13. NUMBER OF PAGES: 34
14. MONITORING AGENCY NAME & ADDRESS (if different from Controlling Office): Office of Naval Research - Boston Branch 666 Summer Street Boston, Massachusetts 02210	15. SECURITY CLASS. (of this report): Unclassified
	15a. DECLASSIFICATION/DOWNGRADING SCHEDULE:

16. DISTRIBUTION STATEMENT (of this Report)

Approved for public release, distribution unlimited.

17. DISTRIBUTION STATEMENT (of the abstract entered in Block 20, if different from Report)

18. SUPPLEMENTARY NOTES

19. KEY WORDS (Continue on reverse side if necessary and identify by block number)

Dimensional Stability	Microcreep
Finite Element Analysis	Micromechanical Properties
Gyroscope Materials	Microstrain Modeling
Hot Isostatically Pressed Beryllium	Microyield Strength
Instrument Materials	

20. ABSTRACT (Continue on reverse side if necessary and identify by block number)

Methods of microyield strength testing are described. The results of microyield strength measurements on hot isostatically pressed beryllium are presented as well as preliminary TEM examination of material in the as-pressed condition.

Error trend data from instrument test is compared to errors predicted from a postulated microcreep law and uniaxial microcreep data. (continued)

DD FORM 1 JAN 73 1473 EDITION OF 1 NOV 65 IS OBSOLETE

UNCLASSIFIED

SECURITY CLASSIFICATION OF THIS PAGE (When Data Entered)

20. Abstract (Continued)

Results of creep analysis on a simple structural shape are presented.

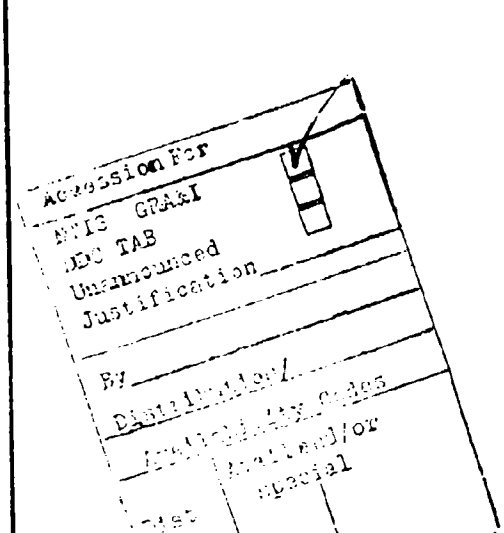

(14) R-1388

MATERIALS RESEARCH FOR ADVANCED INERTIAL INSTRUMENTATION

TASK 1: DIMENSIONAL STABILITY OF GYRO STRUCTURAL MATERIALS

(9) TECHNICAL REPORT NO. 2
FOR THE PERIOD
1 OCTOBER 1978 — 30 SEPTEMBER 1979

JUNE 1980

By

(11) J./McCarthy

F./Petri

Prepared for the Office of Naval Research, Department of the Navy, under Contract (15) N00014-77-C-0388.

APPROVED: M.S. Sapuppo

M.S. Sapuppo, Head
Component Development Department

The Charles Stark Draper Laboratory, Inc.
Cambridge, Massachusetts 02139

ACKNOWLEDGEMENT

This report was prepared by The Charles Stark Draper Laboratory, Inc., under Contract N00014-77-C-0388 with the Office of Naval Research of the Department of the Navy, with Dr. F. S. Gardner of ONR, Boston, serving as Scientific Officer.

TABLE OF CONTENTS

LIST OF ILLUSTRATIONS

LIST OF TABLES

SECTION 1

INTRODUCTION

Dimensional changes in critical components of an instrument will result in errors in the performance of the instrument. The most common sources of such dimensional instability in instruments are: phase transformation, relief of residual stress, and microplastic deformation from applied stresses. Although phase transformation and residual stress may be effectively controlled by proper processing, certain applied stress is essential to the functioning of instruments. The amount of dimensional instability caused by stress can be reduced either by reducing the stress or by increasing the resistance of the material to microplastic deformation. Section 3 of this report is concerned with an investigation of hot isostatically pressed (HIP) beryllium as a material with potentially greater resistance to microplastic deformation than the grades of beryllium currently used in instruments.

As greater demands are made on the accuracy of measuring devices, microplastic strains on the order of 10^{-7} and 10^{-6} become significant sources of instrument error. Strains of this order of magnitude have been found to occur at relatively low stress in moderate strength engineering materials under the action of essential assembly operations such as shrink fit, bolt tension, or rotational stress. Since it is not possible to reduce these assembly stresses below a reasonable limit, it becomes desirable to predict the plastic microstrain and compensate for the resulting errors. Section 4 of this report deals with analytical studies to model the deflection of instrument components as a function of time based on empirical uniaxial microcreep data and finite element stress analysis.

SECTION 2

OBJECTIVES

The principal objectives of this program have been as follows:

(1) To survey the literature on microplastic properties of materials and summarize the data for use in modeling instrument performance and design analysis. This information is contained in the previous year's report.[1]*

(2) To study the microplastic behavior of hot isostatically pressed (HIP) beryllium and the relationship to microstructure.

(3) To predict microdeformation behavior of typical instrument components using finite element analysis techniques and experimentally determined microcreep data.

---

* Superscript numerals refer to similarly numbered items in the List of References.

SECTION 3

THE MICROMECHANICAL BEHAVIOR OF HOT ISOSTATICALLY PRESSED (HIP) BERYLLIUM

3.1 Previous Work

During the first year of this 2-year program, the following was accomplished.

(1) Hot Isostatically pressed beryllium was purchased from Kawecki Berylco Industries. This is their designation HIP50.

(2) A procedure was established for preparing tensile specimens for microyield strength tests and for applying strain gages for measuring microstrain.

(3) Methods for measuring misalignment in loading were investigated and a load train was modified to provide a reasonable value of precision of alignment.

3.2 Present Work

3.2.1 Alignment of Loading

Work was continued on improving the alignment of loading of the test specimen for the microyield strength tests. The squareness and concentricities of the various elements of the load train were inspected and reworked where necessary. A 5-inch-long pull rod with a rod-end bearing was inserted between the specimen holder and the clevis hangers. With this load train design (Figure 1), the typical precision of alignment was 3×10^{-4}. This value corresponds to an extreme fibre bending

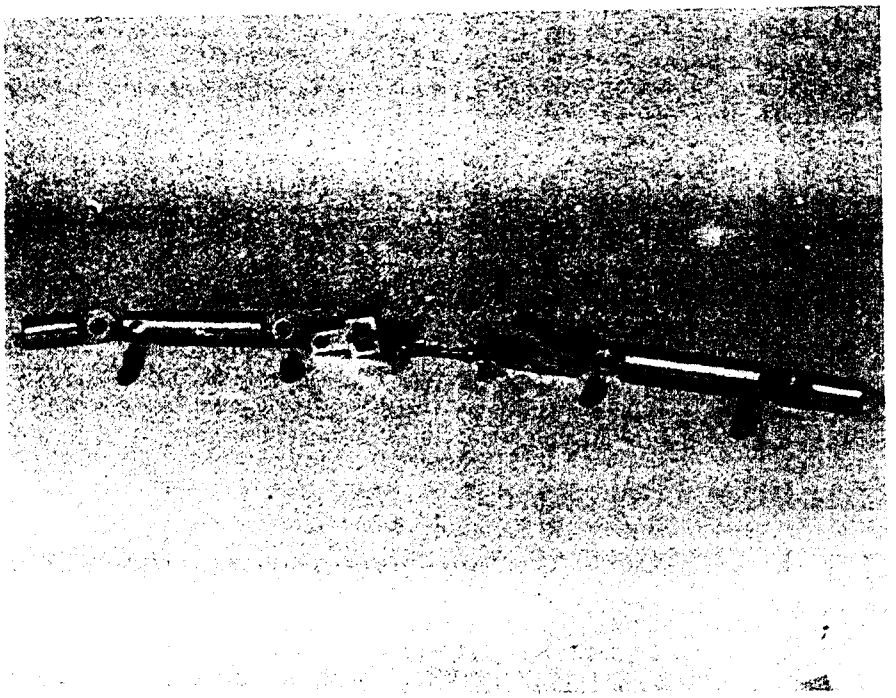

Figure 1. Load Train for microyield strength tests.

stress of 1300 lb/in.^{2} at 5000 lb/in.^{2} average stress. Although this condition can be considered only moderately good alignment, the load train would have to be completely redesigned in order to significantly improve alignment.

3.2.2 Microyield Strength Tests

Microyield strength was determined for HIP50 beryllium in two conditions. The first condition was "as pressed"; the sample was machined and etched only. The second condition consisted of aging at 1080°F for 100 hours. The test specimen preparation and the installation of strain gages has been described previously.[1] The aging treatment was suggested by G. Keith of KBI based on microalloying studies on beryllium at Brush Wellman.[2]

3.2.3 Microyield Strength Testing Methods

The theory and techniques of microyield strength tests have been reviewed extensively by Marschall and Maringer.[3] In the present study, the objective is to define the 1×10^{-6} offset and 2×10^{-6} offset microyield stress using a strain measuring technique which is relatively uncomplicated and which could be adapted to qualification testing.

The apparatus used for conducting microyield stress tests is shown in Figure 2. The instrumented specimen and load train which were previously described are loaded by an Instron tensile machine. The load train is carefully installed in the testing machine to avoid any effects of friction or bending. The lower crosshead is positioned so that the lower pin of the load train is free in the slots of the pull rod (Figure 1) and exerting no force on the train. The tare load on the specimen, which is referred to throughout the test, is the weight on the lower half of the train load.

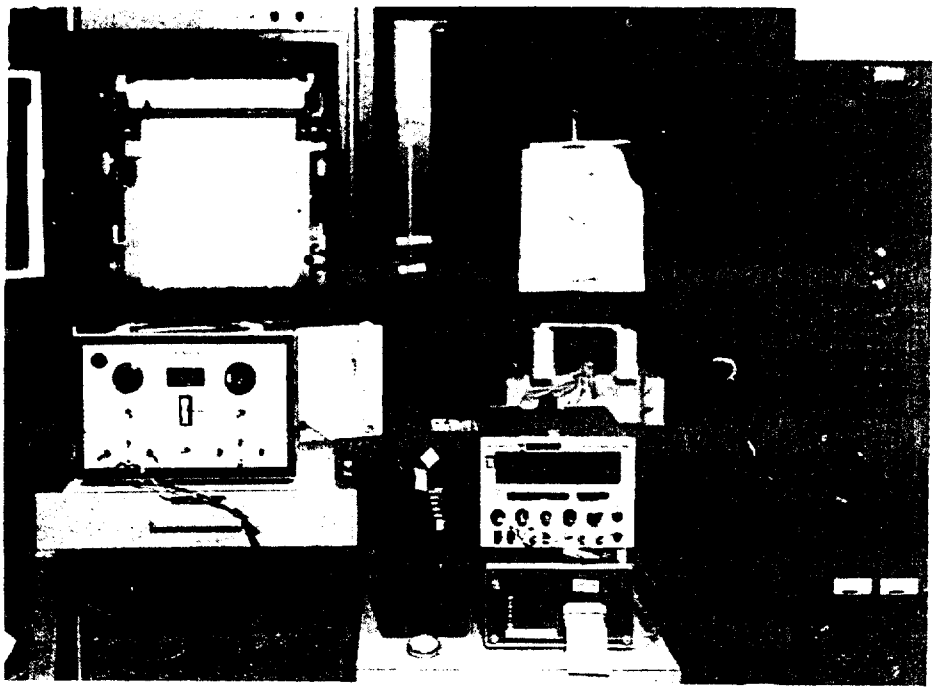

Figure 2. Apparatus for conducting microyield strength tests.

A single strain gage from the three gages on the specimen is connected to the BLH Model 1200 strain indicator. A gage from a dummy unstressed specimen which is hung on the load train is wired with the above active gage for temperature compensation in a half-bridge circuit. Although the strain indicator has a digital readout capability of 1×10^{-6} strain, the sensitivity is increased by installing a BCD output and printing the strain data with a Newport Model 810 Digital Printer. Strain is determined by making 20 consecutive prints from the strain indicator and averaging the values. Printing speed is 2-1/2 prints per second. The specimen and load train are enclosed with a styrofoam enclosure to reduce the effects of room temperature fluctuations.

The other two strain gages on the specimen are connected through a switch box to a second strain indicator and used for determining precision of alignment. Both strain indicators are connected to a General Radio voltage stabilizer.

Before starting a test, the specimen and instrumentation are set up and the instruments allowed to run overnight to establish temperature equilibrium. The specimen is then loaded to a low stress, approximately 2000 $lb/in.^2$, and loaded and unloaded several times to determine the repeatibility of the unstrained zero reading.

The specimen is then loaded and unloaded to increasing values of stress, and the values of loaded and unloaded strain recorded. Strain rate is 0.008 inch/inch/minute loading and unloading. Load is maintained for 30 seconds. When the specimen is fully unloaded, the crosshead is moved at higher speed to establish 0.010-inch clearance between the pin and lower pull rod. After a 1-minute interval, the unloaded strain data is printed out and the specimen reloaded. A typical load-time schematic is shown in Figure 3.

3.2.4 Results of Microyield Strength Tests on HIP50

The stress-residual microstrain plot for specimen 6B (as-pressed) is shown in Figure 4. However, even though the resistance bridge

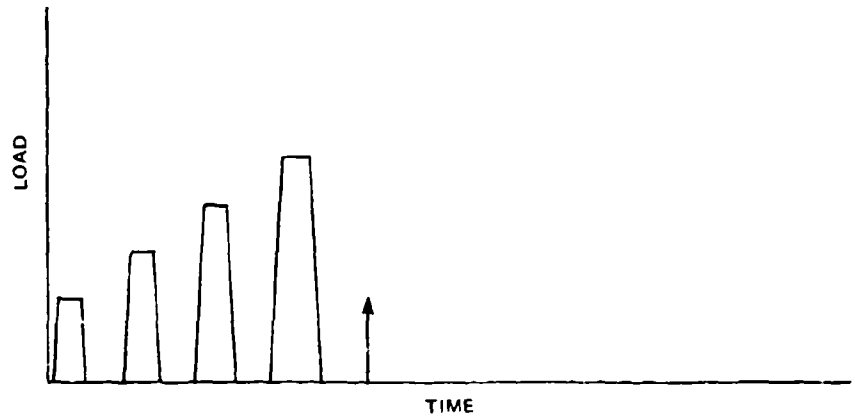

Figure 3. Typical load-time schematic.

formed by the strain gage on the active specimen and the compensating gage on the dummy specimen is self-compensating for temperature, it was found that the strain indicator had a significant error due to changes in room temperature. The specimen temperature is plotted next to the microstrain values to show this effect.

In order to reduce temperature effects on the strain measurements, a temperature controlled enclosure was designed to control the temperature of the specimen and the strain indicator. The apparatus is shown in Figure 5. The enclosure is Plexiglas which is lightly insulated with fiberglass. The air temperature is controlled to ±0.25°F at temperatures of 80 to 85°F. The air is heated by the strain indicator and a small resistance heater which is controlled by a proportional temperature controller. Air flow within the enclosure is by natural convection.

Specimens 3A (as-pressed) and 5A (pressed and aged) were tested with close temperature control. The results are shown in Figures 6 and 7. The strain error from temperature effects has been eliminated and the microyield strength more clearly defined. It can be seen that the aging treatment has produced a significant increase in MYS.

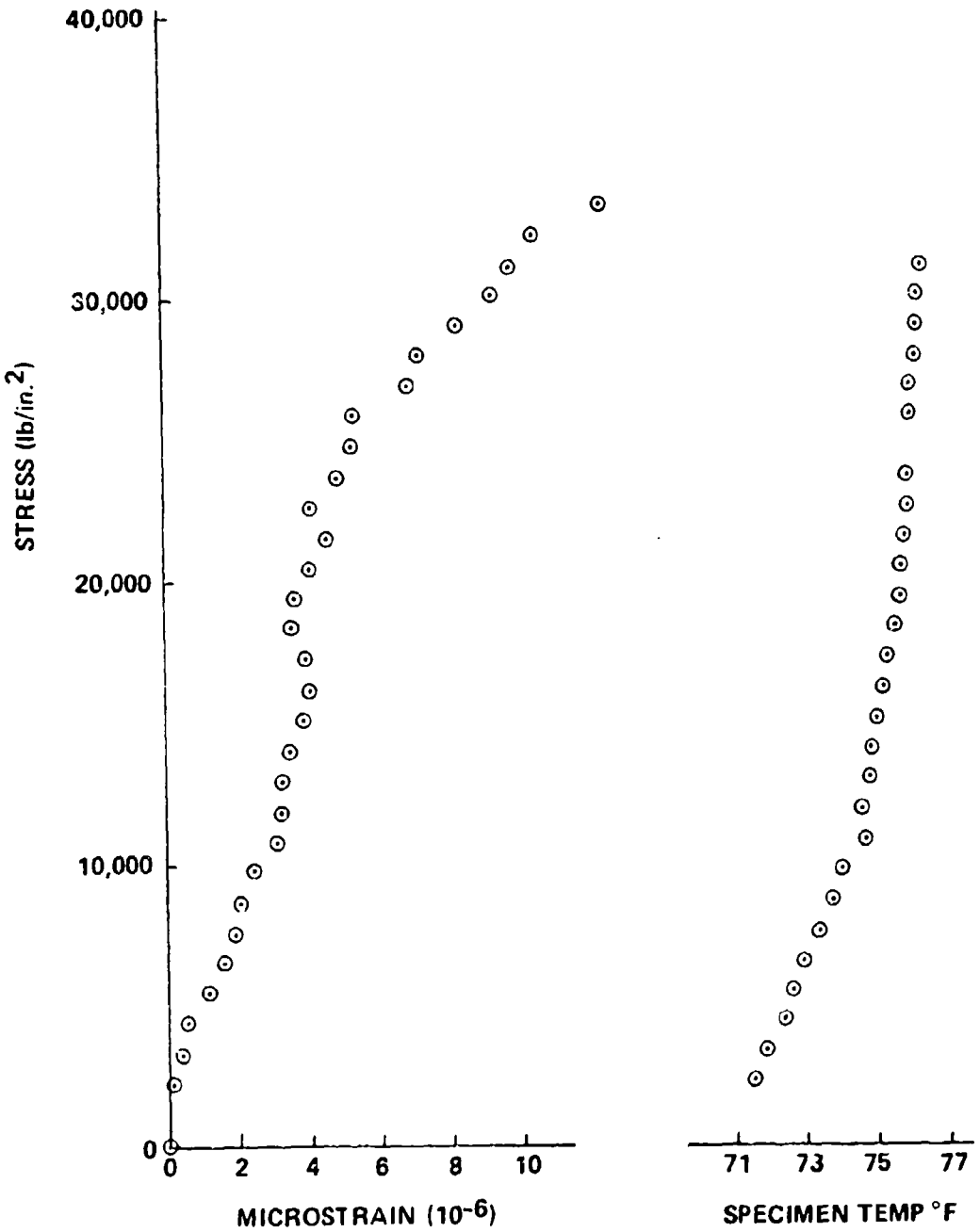

Figure 4. HIP50 beryllium, as-pressed, microyield stress, specimen 6B (temperature as shown).

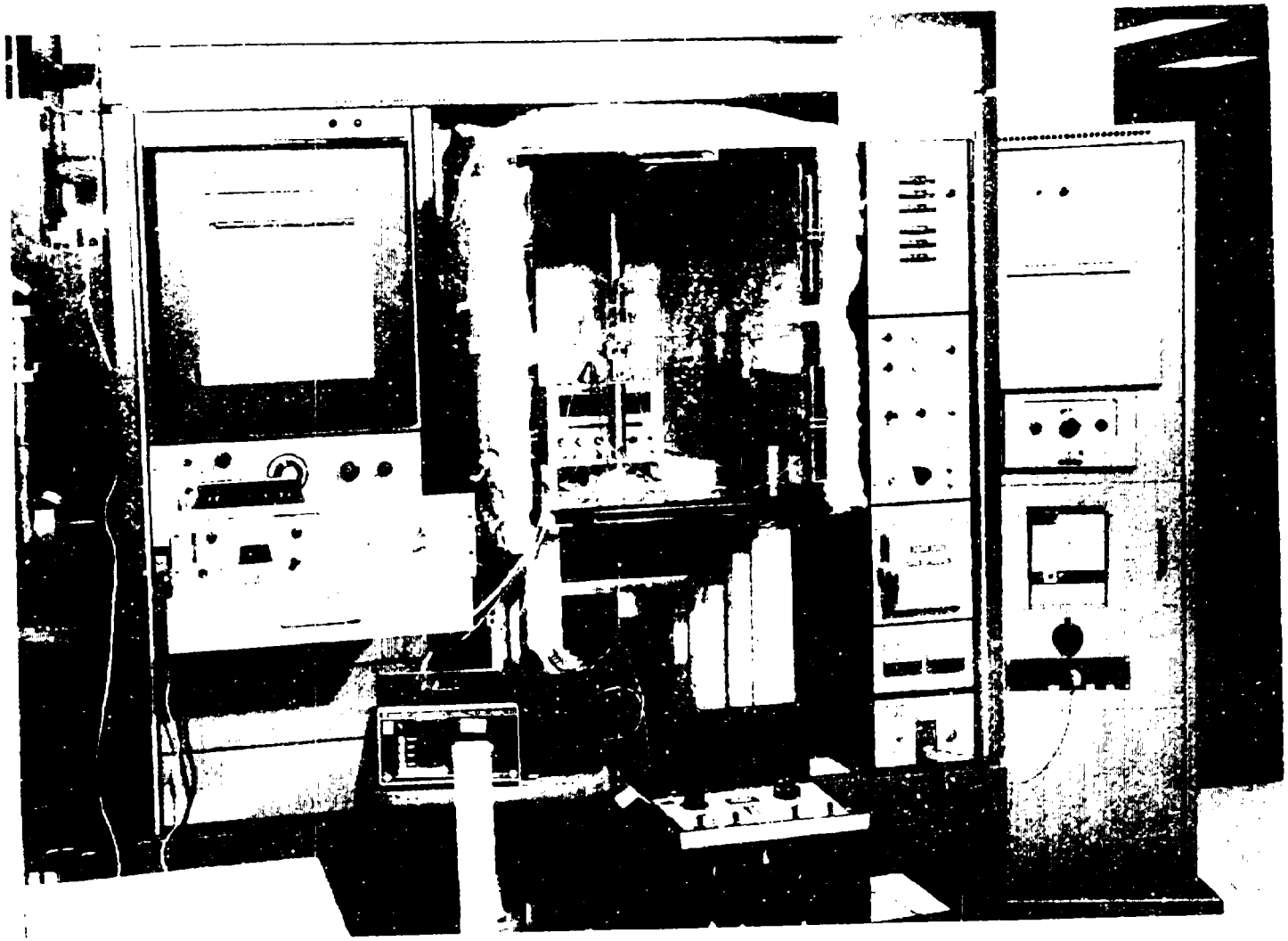

Figure 5. Test setup with temperature controlled enclosure.

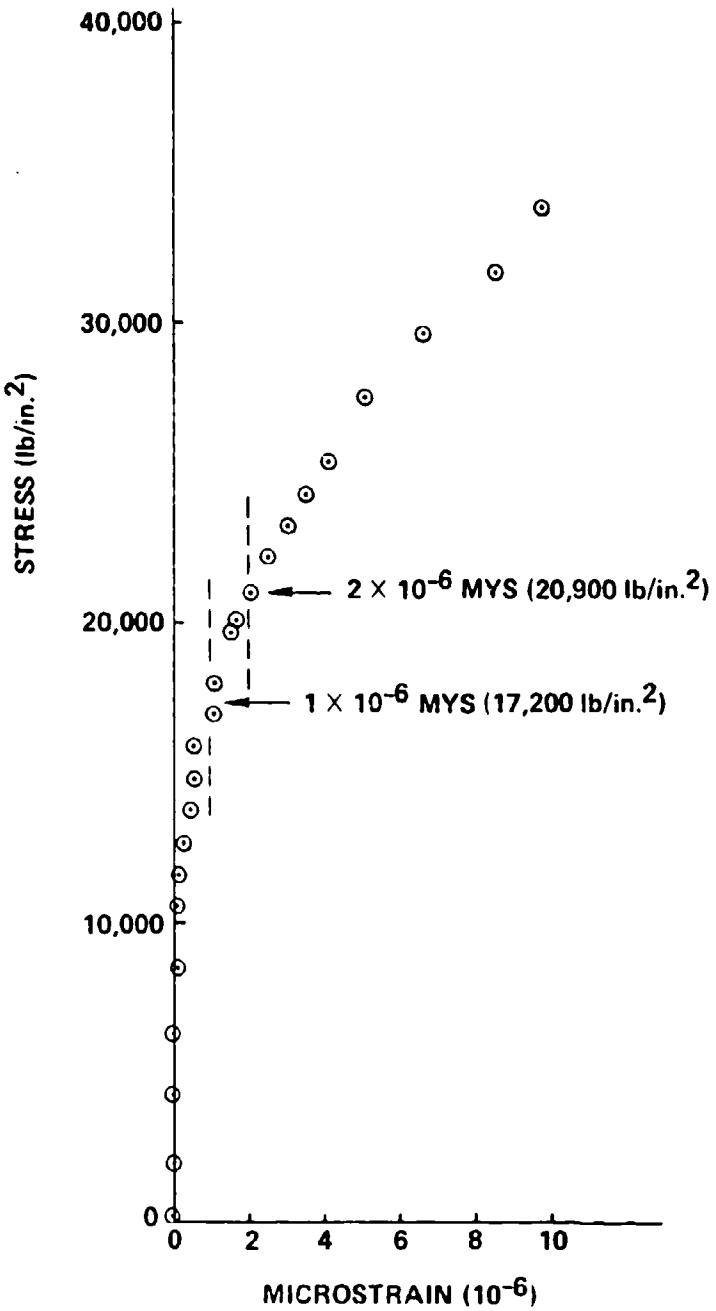

Figure 6. HIP50 beryllium, as-pressed, microyield stress, specimen 3A (temperature—80°F).

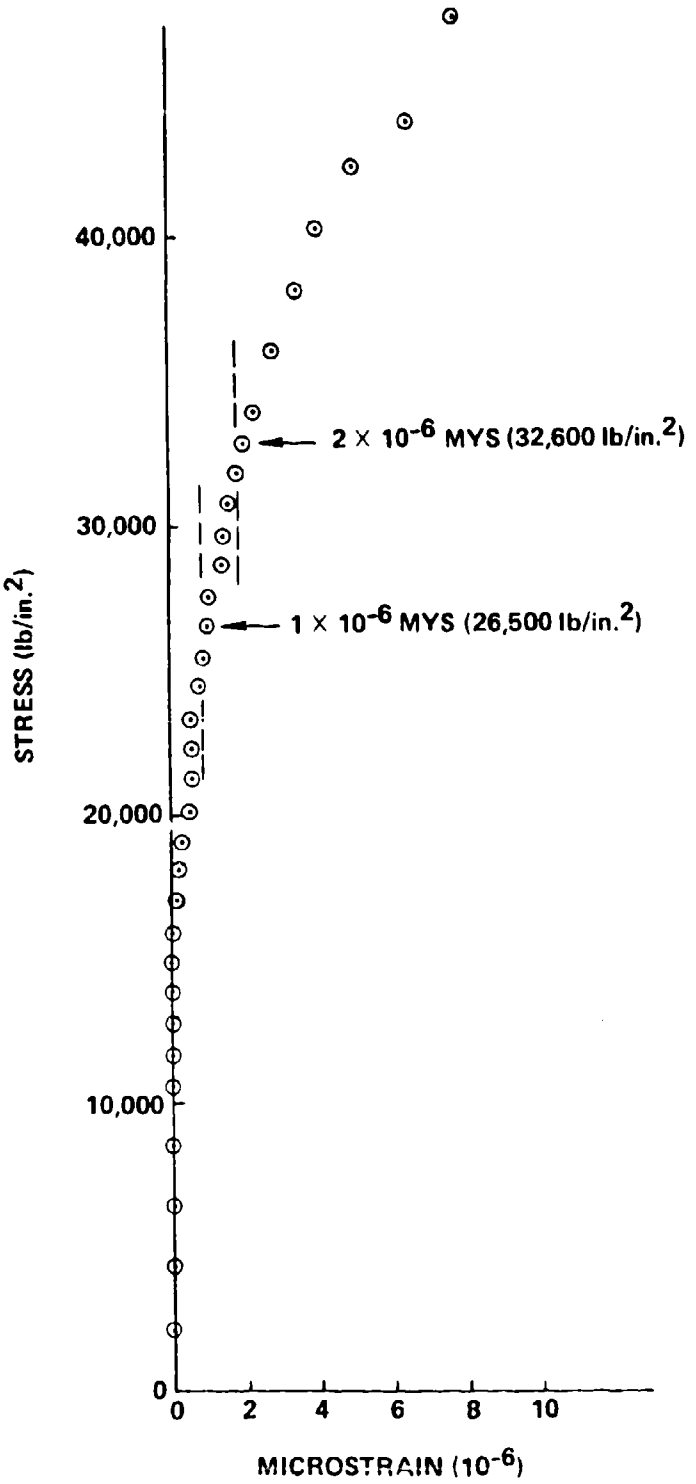

Figure 7. HIP50 beryllium, as-pressed and aged, microyield stress, specimen 5A (temperature—82°F).

3.2.5 Correlation of Microplastic Behavior with Microstructure

One of the objectives of this program is to investigate the relationship between microplastic behavior and microstructure in HIP50. Paine and Stonehouse[2] have found that microalloying reactions between iron, aluminum, and beryllium produce significant changes in mechanical properties, and suggest that similar effects may occur with micromechanical properties. The previously described results of a simple aging treatment with HIP50 beryllium confirms this effect. It would be of great interest to relate the mechanical behavior to microstructural changes.

A preliminary examination of "as-pressed" HIP50 has been made by R. Polvani of National Bureau of Standards using transmission electron microscopy. The preliminary evidence shows that:

(1) There are relatively few agglomerations of BeO in HIP50 but there are numerous small particle colonies (this is shown in Figure 8).

(2) The "as-pressed" material has internal stresses.

(3) The dislocation density is relatively high compared to instrument grade beryllium.

This type of microscopy will be extended to other heat treatments of HIP50 in the next year.

3.3 Plans for Future Work

During the next report period, additional heat treatments which will vary the size, number, and relative amounts of $FeBe_{11}$ and $AlFeBe_4$ precipitates will be investigated. Microyield strength will be measured and more extensive metallography will be undertaken. Attempts will be made to relate microyield stress and microcreep behavior in HIP50.

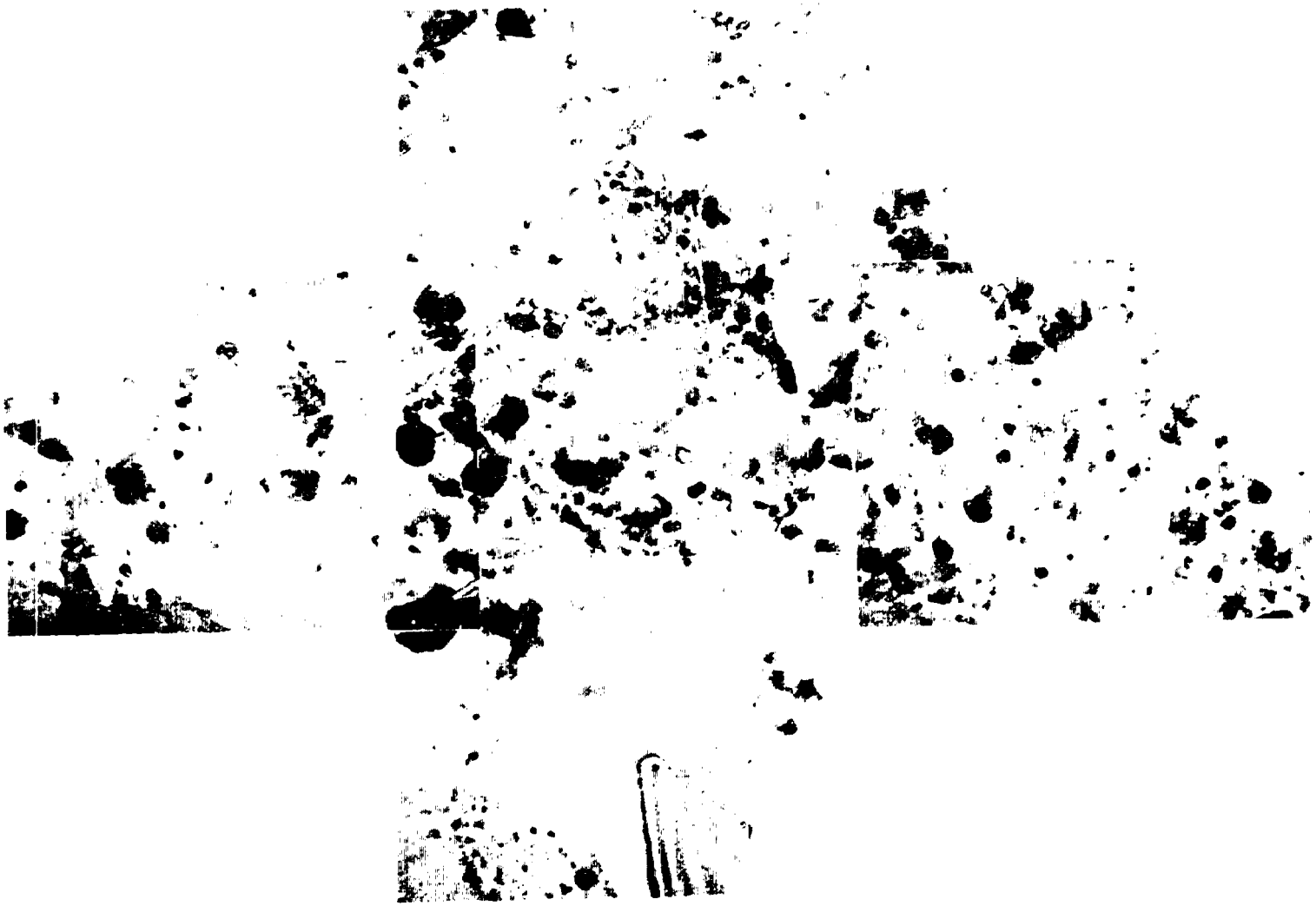

Figure 8. Typical precipitate colony in "as-pressed" HIP50.

SECTION 4

PREDICTION OF MICRODEFORMATION OF TYPICAL INSTRUMENT COMPONENTS

4.1 Correlation of Microcreep Deformation with Instrument Error Trends

4.1.1 Introduction

An instrument which exhibited non-g-sensitive trending was analyzed by applying data from uniaxial test specimens to actual three-dimensional structural instrument parts. Microcreep was correlated with observed error trend data from a typical instrument using a postulated creep law. Since only very limited microcreep data has been available, there is much uncertainty in the creep law used. However, this analysis shows the value of the microcreep tests which are being conducted, and identifies an area of this instrument where design changes can be made to reduce the effect of microcreep.

4.1.2 Trend and Instrument Description

The instrument which was analyzed was a pendulous integrating accelerometer which incorporates a pendulous integrating gyro as part of the overall instrument. Ramps in the scale factors of this group of instruments have been observed with time. Typical plots of these ramps for four instruments are shown in Figures 9 and 10. The ramps are independent of instrument orientation to gravity vector and although the magnitude of scale factors vary somewhat from instrument to instrument, they are consistent in sign. The ramps which are shown could be caused by a shift in the pendulous mass within the gyro. The gyro consists of a

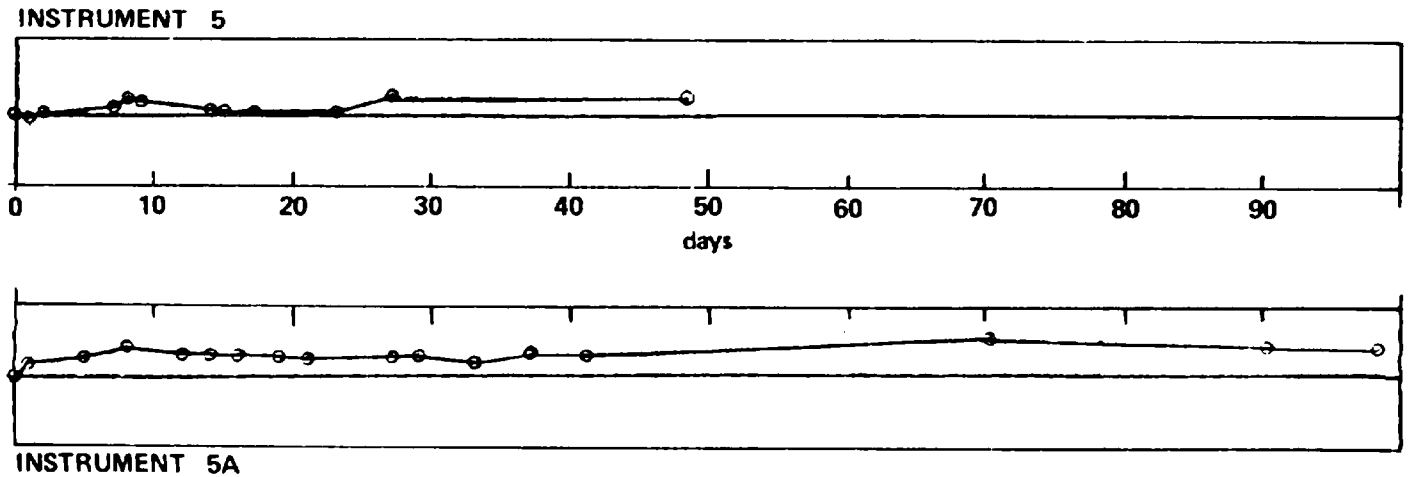

Figure 9. Instrument trend versus time.

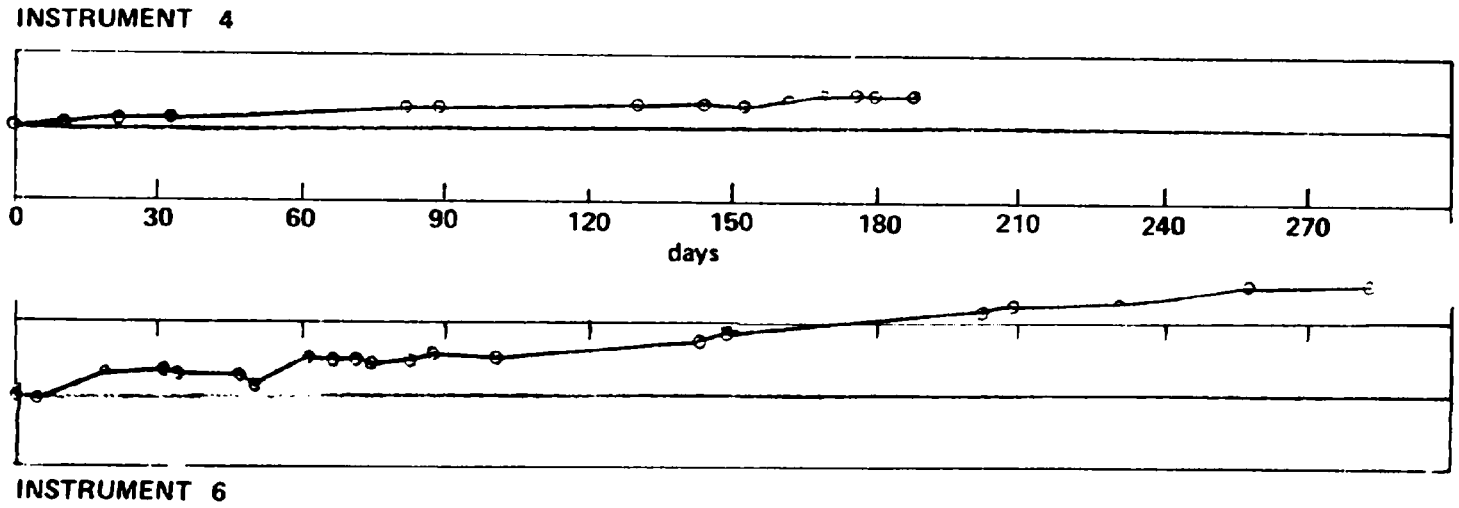

Figure 10. Instrument trend versus time.

spinning wheel on a beryllium shaft supported by cups at each end. One end has an additional thrust plate to resist axial movement. One of the support cups is made of a high density metal (Inconel) to provide pendulosity.

4.1.3 Analysis and Results

Figure 11 shows the structure which was analyzed, as well as the displacements produced by the torque nut loadings on the shaft (displacements magnified 50,000 times). The torque nut loading places the beryllium shaft in tension, and depresses the Inconel support cup. As the beryllium shaft creeps axially, the Inconel cup moves toward its undeflected shape and causes a pendulous mass shift.

The finite element model consists of 37 two-dimensional quadrilateral elements. Compressive and tensile forces produced by the nuts were applied to the shaft and nut elements. The creep law assumed for beryllium is described in Reference (1). The assumed creep law is

$$\Sigma = A\sigma^{n} e^{-\frac{\Delta H}{RT} t}$$

where

Σ = total strain

A = a constant = 123×10^{-6}

σ = uniaxial stress ($lb/in.^2$)

n = stress exponent = 0.25

$\Delta H/R$ = activation constant = 6500

T = absolute temperature (°R)

t = time (hours)

It should be emphasized that this is a very preliminary attempt at a creep law pending further results of the experimental work at NBS.

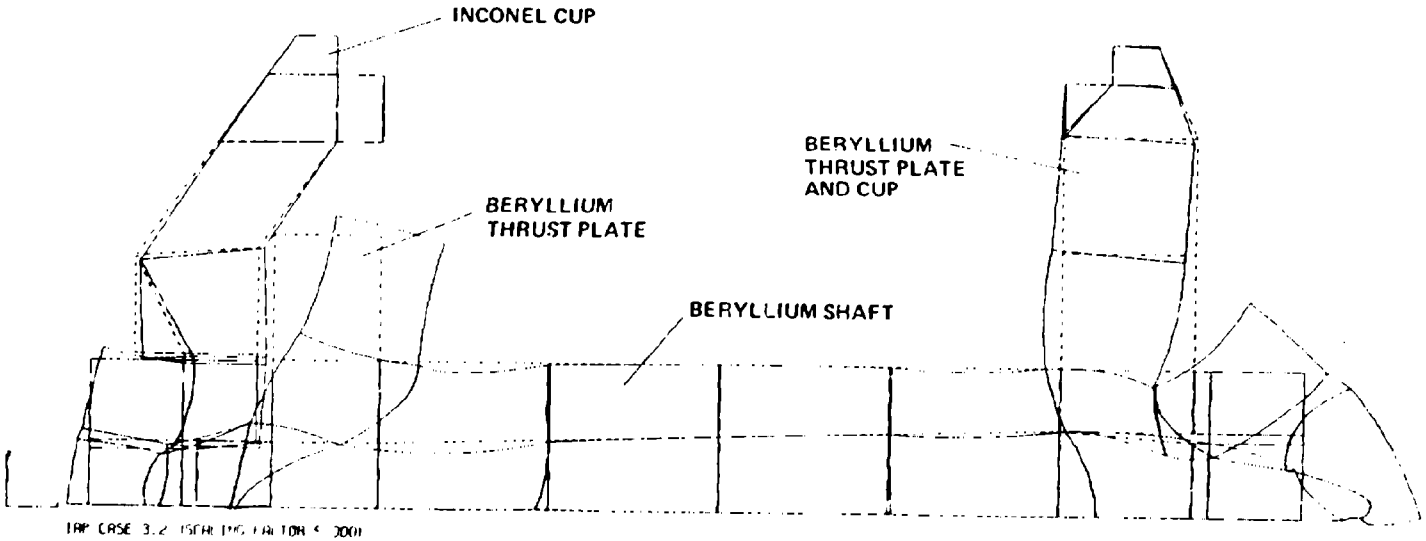

Figure 11. Displacement plot of torque nut loading on beryllium shaft.

However, the results are very interesting in that they indicate there is a strong possibility that the observed trending is caused by microcreep. In fact, using the above law, the predicted microcreep causes about four times the mean trend shown in Figures 9 and 10.

4.2 Analysis of Disc Specimen for Structural Tests

A creep analysis has been conducted in support of the National Bureau of Standards beryllium disc creep test. The test specimen is a 2-inch diameter, 1/8-inch-thick beryllium disc. The following properties were assumed:

$$\text{MODULUS OF ELASTICITY } (E) = 42 \times 10^6 \text{ lb/in.}^2$$

$$\text{DENSITY } (\rho) = 0.07 \text{ lb/in.}^3$$

$$\text{POISSON'S RATIO } (\mu) = 0.025$$

The MARC structural analysis program was used to perform the analysis. The support and loading conditions used in the analysis are shown in Figure 12.

Because of the axisymmetric support and loading conditions, the finite element model of the disc was assembled, as shown in Figure 13, using 8 node axisymmetric quadrilateral elements. This is MARC element No. 28.

Two models were constructed, one having 16 elements and the other 128 elements. These are shown in Figures 14 and 15. Test runs were conducted with each of the models. The static analyses calculated the deflection due to a point load P applied as shown in Figure 12. The Z deflection at the center of the disc, on the side opposite the applied load, was within 3 percent of the closed form solution, for both models.

The creep law described in the preceding section was used for this analysis. The total time over which creep occurs was taken to be 2.375 days and the temperature of the test specimen was assumed to be 70°F. The applied load was 1 pound. There were two uncertainties that

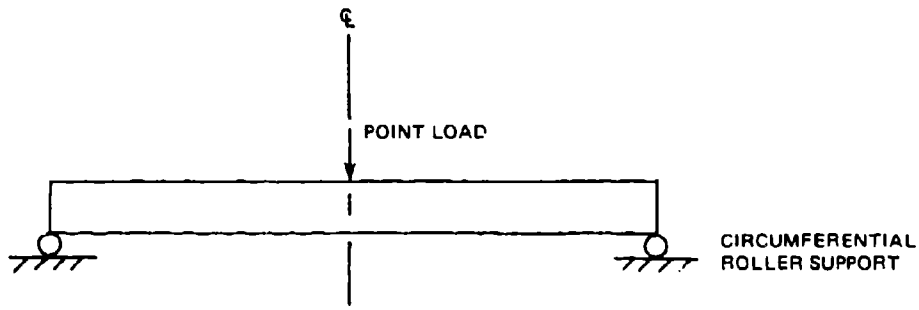

Figure 12. Assumed loading and support of test specimen.

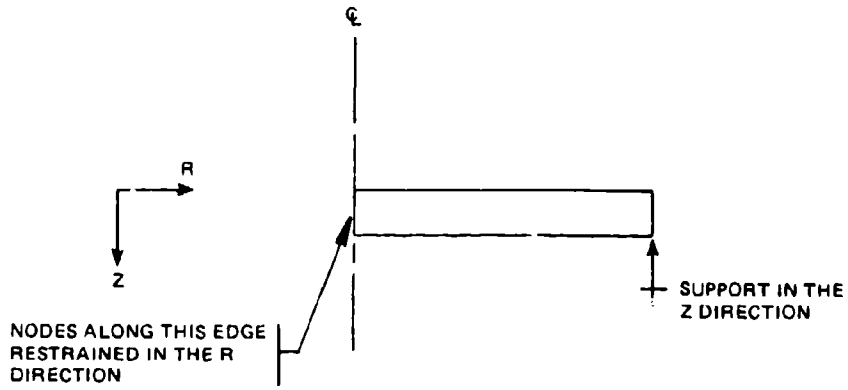

Figure 13. Axisymmetric model.

developed during the analysis. One concerned the effect of the relatively high contact stress that occurs at the point of application of the load, and the other related to the effect of the frictional forces that might develop at the roller support. As a basis of comparison, analysis runs were conducted which included a frictional force in the R direction at the support. The coefficient of friction was assumed to be 0.50.

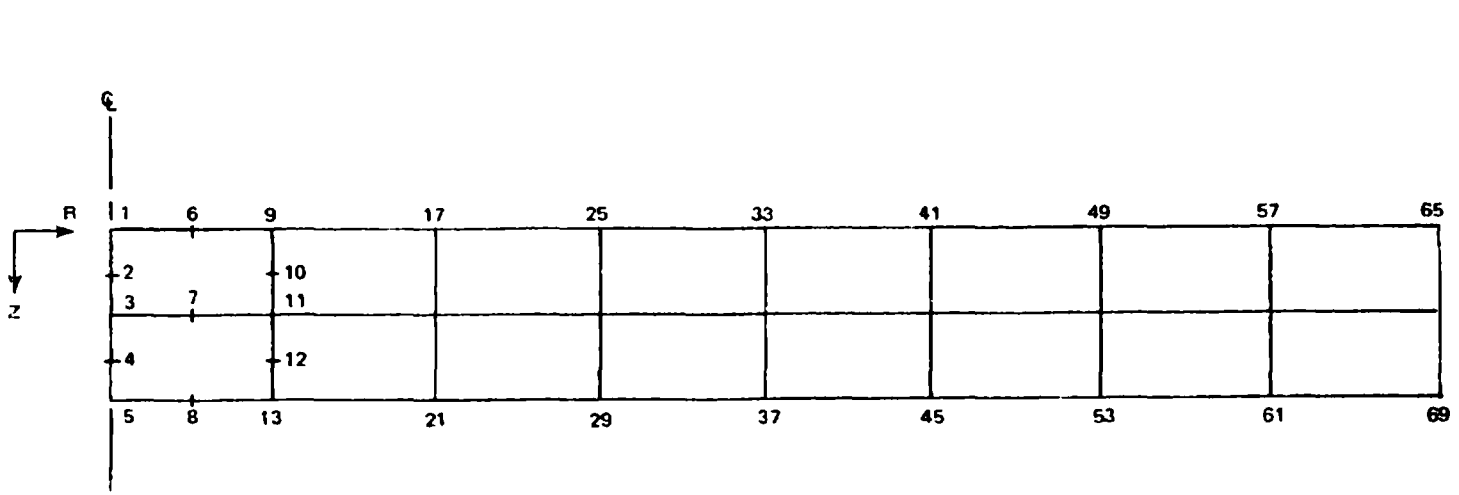

Figure 14. 16-element axisymmetric model.

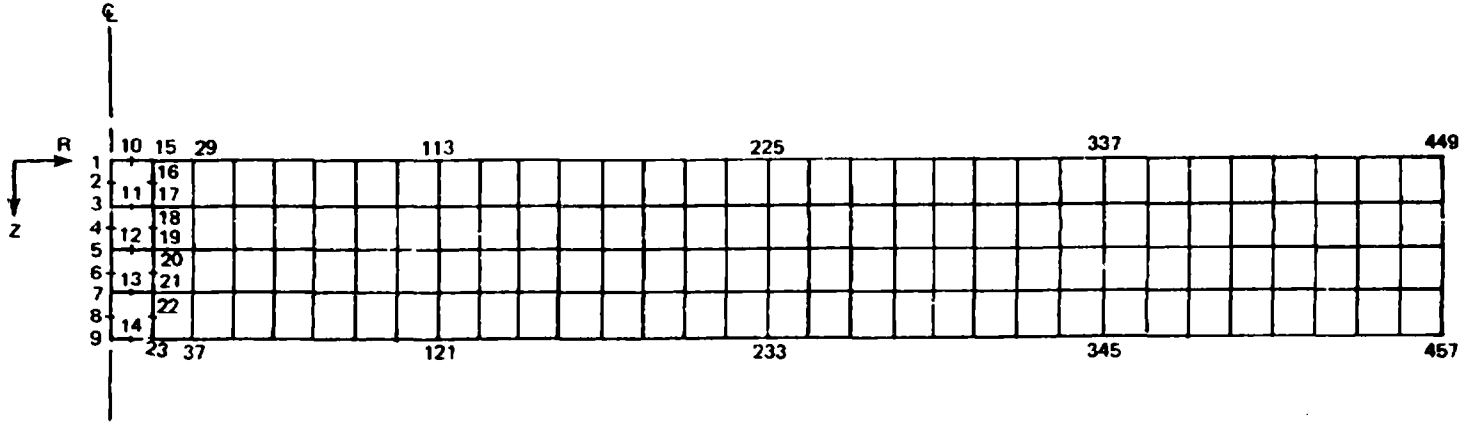

Figure 15. 128-element axisymmetric model.

This was done for both the 16-element structural model and the 128-element model; the finer model was used to assess the effects on the test measurements of the higher stresses in the area where the load is applied. Table 1 shows the results of these analyses. The nodes of interest are those on the side of the disc opposite to where the load will be applied. This is where the test measurements will be made. Inspection of the results shown in columns 4 and 8 indicates that there should be no problem provided reasonable care is taken to eliminate friction at the roller support. The results in columns 9 and 10 show that the 16-element model is quite adequate. This is a favorable result since the 16-element model can be analyzed at approximately one-tenth the cost of the 128-element model for comparable creep analysis runs.

Table 1. Vertical deflections after 2375 days of creep (1-lb load at center of disc).

① Node No. 16-Element Model	② Deflection, Roller Support (in.)	③ Deflection Friction ϕ Support (in.)	④ % Difference 2 vs 3	⑤ Node No. 12d-Element Model	⑥ Deflection, Roller Support (in.)	⑦ Deflection Friction ϕ Support (in.)	⑧ % Difference 6 vs 7	Model Comparison	
								⑨ % Difference 2 vs 6	⑩ % Difference 3 vs 7
1	9.9399E-6	9.5773E-6	3.65	1	1.1366E-5	1.1001E-5	3.21	14.35	14.87
5	9.4384E-6	9.0759E-6	3.84	9	9.4554E-6	9.0896E-6	3.87	0.18	0.15
17	8.2005E-6	7.8593E-6	4.16	113	8.2136E-6	7.8693E-6	4.19	0.16	0.13
21	8.2009E-6	7.8600E-6	4.16	121	8.2136E-6	7.8695E-6	4.19	0.15	0.12
33	5.8698E-6	5.5947E-6	4.69	225	5.8816E-6	5.6033E-6	4.73	0.20	0.15
37	5.8698E-6	5.5950E-6	4.68	233	5.8816E-6	5.6036E-6	4.73	0.20	0.15
49	3.0290E-6	2.8661E-6	5.38	337	3.0400E-6	2.8739E-6	5.46	0.36	0.27
53	3.0290E-6	2.8665E-6	5.36	345	3.0400E-6	2.8743E-6	5.46	0.36	0.27
65	1.5057E-8	1.1639E-8	22.7	449	2.5039E-8	1.8195E-8	27.33	66.29	56.33
69	0	0	0	457	0	0	0	0	0

LIST OF REFERENCES

1. McCarthy, J., and F. Petri, Materials Research for Advanced Inertial Instrumentation, Task 1: Dimensional Stability of Gyro Structural Materials, Charles Stark Draper Laboratory Report R-1231, September 1978.

2. Paine, R.M., and A.J. Stonehouse, Investigation Into Effects of Micro-alloying and Thermal Treatment on the Properties of Beryllium, Final Report on Contract N60921-72-C-0284, Report BW-TR-549, Brush Wellman Inc., Cleveland, Ohio, 44110, 1974.

3. Marschall, C.W., and R.E. Maringer, Dimensional Instability, An Introduction, Pergamon Press, Oxford, 1977.

BASIC DISTRIBUTION LIST

ORGANIZATION	COPIES
Defense Documentation Center Cameron Station Alexandria, VA 22314	12
Office of Naval Research Department of the Navy 800 N. Quincy Street Arlington, VA 22217	1
ATTN: Code 471	1
Code 102	1
Code 470	1
Commanding Officer Office of Naval Research Branch Office Building 114, Section D 666 Summer Street Boston, MA 02210	1
Commanding Officer Office of Naval Research Branch Office 536 South Clark Street Chicago, IL 60605	1
Office of Naval Research San Francisco Area Office 760 Market Street, Room 447 San Francisco, CA 94102	1
Naval Research Laboratory Washington, DC 20375	
ATTN: Code 6000	1
Code 6100	1
Code 6300	1
Code 6400	1
Code 2627	1
Naval Air Development Center Code 302 Warminster, PA 18964 ATTN: Mr. F. S. Williams	1

ORGANIZATION	COPIES
Naval Air Propulsion Test Center Trenton, NJ 08628 ATTN: Library	1
Naval Construction Battalion Civil Engineering Laboratory Port Hueneme, CA 93043 ATTN. Materials Division	1
Naval Electronics Laboratory San Diego, CA 92152 ATTN: Electron Materials Sciences Division	1
Naval Missile Center Materials Consultant Code 3312-1 Point Mugu, CA 92041	1
Commanding Officer Naval Surface Weapons Center White Oak Laboratory Silver Spring, MD 20910 ATTN: Library	1
David W. Taylor Naval Ship Research and Development Center Materials Department Annapolis, MA 21402	1
Naval Undersea Center San Diego, CA 92132 ATTN: Library	1
Naval Underwater System Center Newport, RI 02840 ATTN: Library	1
Naval Weapons Center China Lake, CA 93555 ATTN: Library	1
Naval Postgraduate School Monterey, CA 93940 ATTN: Mechanical Engineering Department	1

BASIC DISTRIBUTION LIST (continued)

ORGANIZATION	COPIES
Naval Air Systems Command Washington, DC 20360 ATTN: Code 52031 Code 52032	 1 1
Naval Sea System Command Washington, DC 20362 ATTN: Code 035	1
Naval Facilities Engineering Command Alexandria, VA 22331 ATTN: Code 03	1
Scientific Advisor Commandant of the Marine Corps Washington, DC 20380 ATTN: Code AX	1
Naval Ship Engineering Center Department of the Navy Washington, DC 20360 ATTN: Code 6101	1
Army Research Office P.O. Box 12211 Triangle Park, NC 27709 ATTN: Metallurgy and Ceramics Program	1
Army Materials and Mechanics Research Center Watertown, MA 02172 ATTN: Research Programs Office	1
Air Force Office of Scientific Research Bldg. 410 Bolling Air Force Base Washington, DC 20332 ATTN: Chemical Science Directorate Electronics and Solid State Sciences Directorate	1

ORGANIZATION	COPIES
NASA Headquarters Washington, DC 20546 ATTN: Code RRM	1
NASA (216) 433-4000 Lewis Research Center 21000 Brookpark Road Cleveland, OH 44135 ATTN: Library	1
National Bureau of Standards Washington, DC 20234 ATTN: Metallurgy Division Inorganic Materials Division	1
Director Applied Physics Laboratory University of Washington 1013 Northeast Fortieth Street Seattle, WA 98105	1
Defense Metals and Ceramics Information Center Battelle Memorial Institute 505 King Avenue Columbus, OH 43201	1
Metals and Ceramics Division Oak Ridge National Laboratory P.O. Box X Oak Ridge, TN 37380	1
Los Alamos Scientific Laboratory P.O. Box 1663 Los Alamos, NM 87544 ATTN: Report Librarian	1
Argonne National Laboratory Metallurgy Division P.O. Box 229 Lemont, IL 60439	1

BASIC DISTRIBUTION LIST (continued)

ORGANIZATION	COPIES
Air Force Materials Laboratory Wright-Patterson AFB Dayton, OH 45433	1
Library Building 50, Rm 134 Lawrence Radiation Laboratory Berkeley, CA	1
Brookhaven National Laboratory Technical Information Division Upton, Long Island New York 19973 ATTN: Research Library	1
Office of Naval Research Branch Office 1030 East Green Street Pasadena, CA 91106	1

SUPPLEMENTARY DISTRIBUTION LIST

Dr. Bruce W. Christ
Division 562
National Bureau of Standards
325 S. Broadway
Boulder, CO 80303

Dr. Robert S. Polvani
Room B-120, Materials Bldg.
National Bureau of Standards
Washington, D.C. 20234

Dr. A. W. Ruff, Jr.
National Measurement Laboratory
National Bureau of Standards
Washington, DC 20234

Dr. Robert Hocken
Room B-104, Metrology Bldg.
National Bureau of Standards
Washington, D.C. 20234

Dr. Gilbert J. London
Code 2023
Naval Air Development Center
Warminster, PA 18974

Professor G. S. Ansell
Rensselaer Polytechnic Institute
Dept. of Metallurgical Engineering
Troy, NY 12181

Professor J. B. Cohen
Northwestern University
Dept. of Material Sciences
Evanston, IL 60201

Professor M. Cohen
Massachusetts Institute of Technology
Department of Metallurgy
Cambridge, MA 02139

Professor J. W. Morris, Jr.
University of California
College of Engineering
Berkeley, CA 94720

Professor O. D. Sherby
Stanford University
Materials Sciences Division
Stanford, CA 94300

Dr. E. A. Starke, Jr.
Georgia Institute of Technology
School of Chemical Engineering
Atlanta, GA 30332

Professor David Turnbull
Harvard University
Division of Engineering and
Applied Physics
Cambridge, MA 02139

Dr. D. P. H. Hasselman
Montana Energy and MHD Research
and Development Institute
P.O. Box 3809
Butte, MT 59701

Dr. L. Hench
University of Florida
Ceramics Division
Gainesville, FL 32601

Dr. J. Ritter
University of Massachusetts
Department of Mechanical Engineering
Amherst, MA 01002

Professor G. Sines
University of California, Los Angeles
Los Angeles, CA 90024

Director
Materials Sciences
Defense Advanced Research Projects
Agency
1400 Wilson Boulevard
Arlington, VA 22209

Professor H. Conrad
University of Kentucky
Materials Department
Lexington, KY 40506

SUPPLEMENTARY DISTRIBUTION LIST (continued)

Dr. A. G. Evans
Dept. Material Sciences and
Engineering
University of California
Berkeley, CA 94720

Professor H. Herman
State University of New York
Materials Sciences Division
Stoney Brook, NY 11794

Professor J. P. Hirth
Ohio State University
Metallurgical Engineering
Columbus, OH 43210

Professor R. M. Latanision
Massachusetts Institute of Technology
77 Massachusetts Avenue
Room E-19-702
Cambridge, MA 02139

Dr. Jeff Perkins
Naval Postgraduate School
Monterey, CA 93940

Dr. R. P. Wei
Lehigh University
Institute for Fracture and
Solid Mechanics
Bethlehem, PA 18015

Professor H. G. F. Wilsdorf
University of Virginia
Department of Materials Science
Charlottesville, VA 29903

Mr. Robert C. Fullerton-Batten
Kawecki Berylco Industries, Inc.
P.O. Box 1462
Reading, PA 19603

Mr. Norman Pinto
Kawecki Berylco Industries, Inc.
P.O. Box 1462
Reading, PA 19603

A. G. Gross
Mechanical Metallurgy Unit
Autonetics, Inc.
Anaheim, CA

A. J. Stonehouse
The Brush Beryllium Co.
Cleveland, OH

C. W. Marschall
Columbus Laboratories
Battelle Memorial Institute
Columbus, OH

R. E. Maringer
Columbus Laboratories
Battelle Memorial Institute
Columbus, OH

J. E. Hanafee
Lawrence Livermore Laboratory
University of California
Livermore, CA 94550

Dr. Frank Gardner
Acting Scientific Director
Office of Naval Research
Building 114-Section D
666 Summer Street
Boston, MA 02210

Dr. Phil Clarkin
Metallurgy and Ceramics
Office of Naval Research
6th Floor, Room 619
800 N. Quincy Street
Arlington, VA 22217

SUPPLEMENTARY DISTRIBUTION LIST (continued)

Mr. George Keith
Kawecki Berylco Industries, Inc.
P.O. Box 1462
Reading, PA 19603

Mr. Bruce Borchardt
Room B-104, Metrology Bldg.
National Bureau of Standards
Washington, D C. 20234

Mr. Tom Charlton
Room B-104, Metrology Bldg.
National Bureau of Standards
Washington, D.C. 20234